Int. J. Heat Mass Transfer. Vol. 15, pp. 1819–1836. Pergamon Press 1972. Printed in Great Britain

BUOYANCY EFFECTS ON LAMINAR HEAT TRANSFER IN THE THERMAL ENTRANCE REGION OF HORIZONTAL RECTANGULAR CHANNELS WITH UNIFORM WALL HEAT FLUX FOR LARGE PRANDTL NUMBER FLUID

K. C. CHENG, S. W. HONG and G. J. HWANG*

Department of Mechanical Engineering, University of Alberta, Edmonton, Alberta, Canada

(*Received* 6 *October* 1971 *and in revised form* 6 *December* 1971)

Abstract—The Graetz problem for fully developed laminar flow in horizontal rectangular channels with uniform wall heat flux is extended by including buoyancy effects in the analysis for the case of large Prandtl number fluid. A general formulation valid for all Prandtl numbers is presented and the limiting case of large Prandtl number is approached by a numerical method. The typical developments of temperature profile, wall temperature and secondary flow in the thermal entrance region are presented for the case of square channel $\gamma = 1$. Local Nusselt number variations are presented for the aspect ratios $\gamma = 0{\cdot}2$, $0{\cdot}5$, 1, 2 and 5 with Rayleigh number as parameter. Due to entry and secondary flow effects, a minimum Nusselt number occurs at some distance from the entrance, depending on the magnitude of Rayleigh number. This behavior is similar to that observed in the thermal entrance region where the transition from laminar to turbulent flow occurs. The effect of Rayleigh number is seen to decrease the thermal entrance length, and the Graetz solution, neglecting buoyancy effects, is found to be applicable only when Rayleigh number is less than about 10^3. A study of the practical implications of large Prandtl number on heat transfer results for hydrodynamically and thermally fully developed case reveals that the present heat transfer results are valid for Prandtl number ranging from order 10 to infinity.

NOMENCLATURE

A, cross-sectional area of a channel;
a, b, width and height of a rectangular channel, respectively;
C, a constant $(D_e^2/\overline{W}_f\mu)\,\partial P_f/\partial Z$;
D_e, equivalent hydraulic diameter, $4A/S$;
Gr, Grashof number, $g\beta\theta_c D_e^3/\nu^2$;
g, gravitational acceleration;
$\bar{h}$, average heat transfer coefficient;
k, thermal conductivity;
M, N, number of divisions in X and Y directions, respectively;
Nu, local Nusselt number, $\bar{h}D_e/k$;
n, outward normal direction to the wall;
P, P_f, pressure deviation and pressure for fully developed laminar flow before thermal entrance, respectively;
p, p_f, dimensionless quantities for P and P_f, respectively;
q_w, uniform heat flux at wall;
Pr, Prandtl number, ν/κ;
Ra, Rayleigh number, $PrGr$;
Re, Reynolds number, $\overline{W}_f D_e/\nu$;
S, circumference of cross-section;
T, temperature;
T_0, uniform fluid temperature at entrance;
U, V, W, velocity components in X, Y, Z directions due to buoyancy effect;
u, v, w, dimensionless quantities for U, V and W;

* Present address: Department of Mechanical Engineering, Cheng Kung University, Tainan, Taiwan, China.

W_f, fully developed axial velocity before thermal entrance;
w_f, dimensionless quantity for W_f;
X, Y, Z, rectangular coordinates;
x, y, z, dimensionless rectangular coordinates.

Greek letters
β, coefficient of thermal expansion;
γ, aspect ratio of a rectangular channel, a/b;
ε, a prescribed error defined by equation (18);
θ, dimensionless temperature difference, $(T - T_0)/\theta_c$;
θ_c, characteristic temperature, $q_w D_e/k$;
κ, thermal diffusivity;
μ, viscosity;
ν, kinematic viscosity;
ξ, vorticity, $\nabla^2\psi$;
ρ, density;
ψ, dimensionless stream function.

Subscripts
b, bulk temperature;
c, characteristic quantity;
f, fully developed quantity before thermal entrance;
i, j, space subscripts of grid point in X and Y directions;
n, an integer defined by equation (19);
w, value at wall;
0, value for pure forced convection.

Superscripts
n, nth iteration or an integer identifying the axial location;
$\bar{}$, average value.

1. INTRODUCTION

SINCE the publication of Graetz's classical work [1] on thermal entrance region heat transfer for fully developed laminar flows in tubes with uniform wall temperature, the Graetz problem has been extended in many ways, particularly in recent years. The common assumption of constant physical properties for Graetz problem leads to pure forced convection problem and an analytical solution [2] is available for the generalized Graetz problem considering the axial conduction effect and employing the rigorous thermal boundary condition of uniform fluid temperature at $Z = -\infty$ rather than at entrance $Z = 0$ where a step change in wall heat flux is imposed. The importance of free convection effect in laminar forced convection has led to many theoretical investigations on fully developed combined free and forced convection in vertical or horizontal tubes. However, the assumption of fully established profiles can be fulfilled only if the channel is very long. In practice, the thermal entrance region heat transfer is of importance, and many experimental investigations have been reported in the literature in recent years. In spite of its practical importance, heretofore, no theoretical solution is available, for example, for Graetz problem with significant buoyancy effects in horizontal tubes or channels because of its mathematical difficulty. The experimental correlation for combined free and forced laminar convection heat transfer in thermal entrance region is further complicated by the temperature-dependent viscosity effect and the most recent correlation [3] based on available experimental data for horizontal isothermal tubes using various fluids still remains to be improved further.

Recent theoretical studies [4, 5] on fully developed combined free and forced laminar convection in uniformly heated horizontal tubes clearly indicate that the inertia terms in both the momentum equation for secondary flow and the axial momentum equation can be neglected for large Prandtl number fluids. With this formulation, the Graetz problem with significant buoyancy effects can now be approached at least by finite-difference technique.

The purpose of this investigation is to study the effect of buoyancy on Graetz problem in

horizontal rectangular channels having aspect ratios 0·2, 0·5, 1, 2 and 5 with uniform wall heat flux for large Prandtl number fluids. The assumption of hydrodynamically fully developed laminar flow in the channel for the Graetz problem is not considered to be very restrictive since for high Prandtl number fluids the velocity profiles develop more rapidly than the temperature profiles. A study of the practical implication of large Prandtl number based on the heat transfer results [4–6] for the case with fully developed thermal and velocity fields suggests that the present formulation based on the asymptotic case of $Pr \to \infty$ is practically valid when the Prandtl number is greater than say order 10.

When the gravitational effect is significant in forced convection, the tube inclination angle or gravitational force orientation effect also arises. It is noted that combined free and forced convection studies are so far limited only to either vertical or horizontal configurations. However, the present formulation and its numerical solution can be extended to the inclined tube case with various thermal boundary conditions.

2. THEORETICAL ANALYSIS

Consideration is given to a steady hydrodynamically fully developed but thermally developing laminar flow of viscous fluid in a horizontal rectangular channel where a step change in uniform wall heat flux is imposed starting at the entrance $Z = 0$ (see Fig. 1). The problem is to determine the temperature development and the variation in heat transfer coefficient along the axial direction using the Boussinesq approximation. The analysis will start with the derivation of the governing equations valid for any Prandtl number. Referring to the coordinate system shown in Fig. 1, the continuity and the complete Navier–Stokes equations become

$$\frac{\partial U}{\partial X} + \frac{\partial V}{\partial Y} + \frac{\partial}{\partial Z}(W_f + W) = 0 \qquad (1)$$

$$U\frac{\partial U}{\partial X} + V\frac{\partial U}{\partial Y} + (W_f + W)\frac{\partial U}{\partial Z} = -\frac{1}{\rho}\frac{\partial}{\partial X}(P_f + P) + \nu\nabla^2_{X,Y,Z}U \qquad (2)$$

$$U\frac{\partial V}{\partial X} + V\frac{\partial V}{\partial Y} + (W_f + W)\frac{\partial V}{\partial Z} = -\frac{1}{\rho}\frac{\partial}{\partial Y}(P_f + P) + \nu\nabla^2_{X,Y,Z}V + g\beta(T - T_0) \qquad (3)$$

$$U\frac{\partial}{\partial X}(W_f + W) + V\frac{\partial}{\partial Y}(W_f + W) + (W_f + W)\frac{\partial}{\partial Z}(W_f + W) = -\frac{1}{\rho}\frac{\partial}{\partial Z}(P_f + P) + \nu\nabla^2_{X,Y,Z}(W_f + W) \qquad (4)$$

$$\frac{1}{\rho}\frac{\partial P_f}{\partial Z} = \nu\nabla^2_{X,Y}W_f \qquad (5)$$

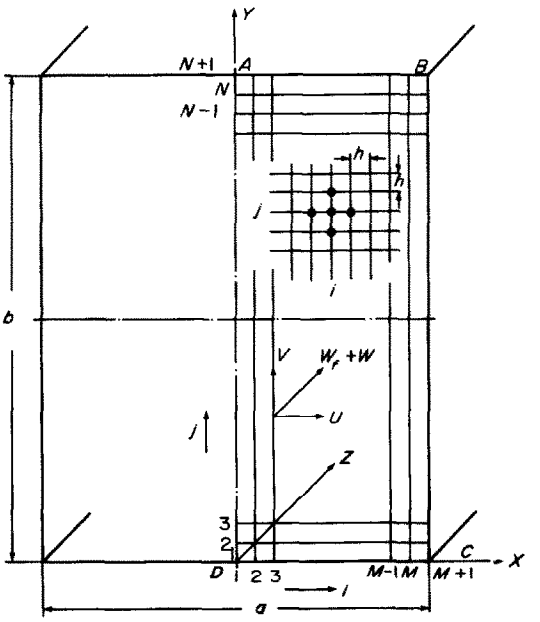

FIG. 1. Coordinate system and numerical grid for horizontal rectangular channel.

where the subscript f indicates the fully developed flow quantity before entering the heated section, W and P the axial velocity and pressure deviations, respectively, in the thermal entrance region, T_0 the reference temperature representing the uniform temperature of the fluid at the entrance $Z = 0$, $\nabla^2_{X,Y,Z} = \partial^2/\partial X^2 + \partial^2/\partial Y^2 + \partial^2/\partial Z^2$, and $\nabla^2_{X,Y} = \partial^2/\partial X^2 + \partial^2/\partial Y^2$. For fully developed flow, one has $\partial W_f/\partial Z = 0$, $\partial P_f/\partial X = 0$, and $\partial P_f/\partial Y = 0$. The buoyant force term which results from temperature differences measured from the reference temperature T_0 is added in the momentum equation in the direction of the gravity vector. It should be pointed out that for the classical Graetz problem the buoyancy effect is neglected completely, and only the axial momentum equation (5) remains with equations (1)–(4) vanishing identically.

Assuming that viscous dissipation is negligible, the energy equation for steady laminar flow can be written as

$$U\frac{\partial T}{\partial X} + V\frac{\partial T}{\partial Y} + (W_f + W)\frac{\partial T}{\partial Z} = \kappa\nabla^2_{X,Y,Z}T. \quad (6)$$

After carrying out the order of magnitude analysis and introducing the following dimensionless variables and parameters,

$$X = [D_e]x, \quad Y = [D_e]y, \quad Z = [D_e PrRe]z,$$
$$U = [\kappa/D_e]u, \quad V = [\kappa/D_e]v, \quad W_f = [\overline{W}_f]w_f,$$
$$W = [\overline{W}_f]w, \quad P_f = [P_c]p_f, \quad P = [P_c]p,$$
$$T - T_0 = [\theta_c]\theta, \quad Gr = (g\beta\theta_c D_e^3/\nu^2),$$
$$Pr = (\nu/\kappa), \quad Ra = PrGr, \quad Re = (\overline{W}_f D_e/\nu),$$

where $D_e = (4A/S)$ and $\theta_c = (q_w D_e/k)$, the following normalized governing equations result:

$$\frac{\partial u}{\partial x} + \frac{\partial v}{\partial y} + \frac{\partial w}{\partial z} = 0 \quad (7)$$

$$\frac{\partial^2 u}{\partial x^2} + \frac{\partial^2 u}{\partial y^2} = \frac{\partial p}{\partial x} + \frac{1}{Pr}\left[u\frac{\partial u}{\partial x} + v\frac{\partial u}{\partial y} + (w_f + w)\frac{\partial u}{\partial z}\right] \quad (8)$$

$$\frac{\partial^2 v}{\partial x^2} + \frac{\partial^2 v}{\partial y^2} = \frac{\partial p}{\partial y} + \frac{1}{Pr}\left[u\frac{\partial v}{\partial x} + v\frac{\partial v}{\partial y} + (w_f + w)\frac{\partial v}{\partial z}\right] + Ra\theta \quad (9)$$

$$\frac{\partial^2 w}{\partial x^2} + \frac{\partial^2 w}{\partial y^2} = \frac{1}{Pr}\left[u\frac{\partial}{\partial x}(w_f + w) + v\frac{\partial}{\partial y} \times (w_f + w) + (w_f + w)\frac{\partial w}{\partial z}\right] \quad (10)$$

$$\frac{\partial^2 w_f}{\partial x^2} + \frac{\partial^2 w_f}{\partial y^2} = \frac{D_e^2}{\overline{W}_f}\frac{1}{\mu}\frac{\partial P_f}{\partial Z} = C, \quad C = \text{constant} \quad (11)$$

$$\frac{\partial^2 \theta}{\partial x^2} + \frac{\partial^2 \theta}{\partial y^2} = u\frac{\partial \theta}{\partial x} + v\frac{\partial \theta}{\partial y} + (w_f + w)\frac{\partial \theta}{\partial z}. \quad (12)$$

In the above formulation, the terms $\partial^2 u/\partial z^2$, $\partial^2 v/\partial z^2$, $\partial^2 w/\partial z^2$, and $\partial p/\partial z$ drop out because of large Peclet number assumption. It is known that the effect of axial conduction term in the energy equation can be neglected practically when the value of Peclet number exceeds about 100. The above set of equations represents a formal mathematical formulation of the classical Graetz problem taking the free convection effect into consideration. The boundary conditions are:

$$u = v = w = w_f = 0 \text{ and } \partial\theta/\partial n = 1 \text{ at wall}$$
$$\theta = 0 \quad \text{at entrance } z = 0. \quad (13)$$

The solution of the above set of equations (7)–(12) subjected to the boundary conditions given by equation (13) cannot be approached readily even by numerical method. However, as Prandtl number approaches infinity, considerable simplification of the governing equations results. When Prandtl number is large, all the terms involving Prandtl number vanish completely. In other words, the inertia force terms in the momentum equations disappear. In particular, equation (10) vanishes identically, implying that $w = 0$ and the axial velocity in the thermal entrance region remains to be given by equation (11) for fully developed flow. With $w = 0$, it is

now possible to introduce a stream function ψ and vorticity ξ as

$$u = \frac{\partial \psi}{\partial y}, \quad v = -\frac{\partial \psi}{\partial x}, \quad \nabla^2 \psi = \xi.$$

Furthermore, the pressure terms in equations (8) and (9) can be eliminated by carrying out cross-differentiation and then reducing them to a single equation. The resulting simplified governing equations for large Prandtl number case become

$$\nabla^2 w_f = C \tag{14}$$

$$\nabla^2 \xi = Ra \frac{\partial \theta}{\partial x} \tag{15}$$

$$\nabla^2 \psi = \xi \tag{16}$$

$$\nabla^2 \theta = u \frac{\partial \theta}{\partial x} + v \frac{\partial \theta}{\partial y} + w_f \frac{\partial \theta}{\partial z} \tag{17}$$

where $\nabla^2 = \partial^2/\partial x^2 + \partial^2/\partial y^2$.

The above formulation for large Prandtl number case is based on the study [4, 5] of Prandtl number effect on fully developed laminar forced convection heat transfer with secondary flow for uniformly heated horizontal tubes [6] and curved rectangular channels [7]. In particular, a study of the numerical results reveals that when $Pr \gtrsim 10$, the value for mean axial velocity remains practically unchanged from that of the pure forced convection even with the increase of the characteristic parameter such as $ReRa$ [6]. This means that for large Prandtl number case the secondary flow is rather weak but it plays an important role through the convective terms in the energy equation. This is in contrast to the classical Graetz problem where $u = v = 0$ and the convective terms ($u\ \partial\theta/\partial x + v\ \partial\theta/\partial y$) in energy equation (17) are neglected. In view of the difficulty with the analytical solution for the set of equations (14)–(17) satisfying the boundary conditions given by equation (13), a numerical solution is believed to be the only practical approach for the present problem. It is noted that the determination of the unknown boundary vorticity associated with the vorticity equation (15) is well discussed elsewhere [5, 6].

3. FINITE-DIFFERENCE SOLUTION

Equations (14)–(16) are second-order partial differential equations of elliptic type. The exact analytical solution to the Poisson's equation (14) satisfying the boundary condition $w_f = 0$ at wall is available for the rectangular channel. However, for convenience the implicit alternating-direction method is used for the numerical solution of equation (14). Equations (15) and (16) can be combined into a single vorticity transport equation involving a biharmonic operator by eliminating vorticity ξ. Although an alternating direction method for solving the biharmonic equation is available [8], a computationally stable and simple approach using a combination of boundary vorticity method [5, 6] and line iterative technique is employed in solving two coupled second-order elliptic equations (15) and (16). Without the axial conduction term, the energy equation (17) is of parabolic type and the implicit alternating-direction method [9] is used.

Because of symmetry, it suffices to solve the problem in one-half of the rectangular region such as that shown in Fig. 1. Briefly, the simultaneous solution of the set of equations (14)–(17) consists of the following main steps:

(1) The Poisson's equation (14) for fully developed velocity w_f is solved independently using ADI method [9] by introducing the unsteady term $\partial w_f/\partial t$.

(2) The initial values for secondary velocity components $u_{i,j}$, $v_{i,j}$ and temperature difference $\theta_{i,j}$ are taken to be zero for the terms on the right-hand side of equation (17) and the equation is solved using ADI method.

(3) The value for Rayleigh number is assigned. With $Ra\ \partial\theta/\partial x$ known, equations (15) and (16) are solved using a combination of boundary vorticity method and line iterative technique. The second velocity components $u_{i,j}$, $v_{i,j}$ are then computed from the stream function.

(4) Equation (17) is solved again using ADI method.
(5) The steps (3) and (4) are repeated until the following convergence criterion is satisfied:

$$\varepsilon = \sum_{i,j} |\theta_{i,j}^{(n+1)} - \theta_{i,j}^{(n)}| / \sum_{i,j} |\theta_{i,j}^{(n+1)}| < 10^{-5}. \quad (18)$$

(6) The axial step size Δz is advanced by the following equation which yields a finer step size near the entrance where the axial temperature gradient is expected to be large.

$$(\Delta z)_n = e^{-7+0.1n}, \quad n = 1, 2, \ldots, 49$$
$$(z)_n = \sum_{n=1}^{n} (\Delta z)_n. \quad (19)$$

Since the step size is not uniform for each step, the axial gradient $(\partial\theta/\partial z)^{(n)}$ is evaluated using the following equation obtained by applying the Taylor series expansion.

$$\left(\frac{\partial\theta}{\partial z}\right)^{(n)} = \{(\Delta z)_n^2 \theta^{(n+1)} - (\Delta z)_{n+1}^2 \theta^{(n-1)} - [(\Delta z)_n^2 - (\Delta z)_{n+1}^2] \theta^{(n)}\} / (\Delta z)_{n+1} \times (\Delta z)_n [(\Delta_\zeta)_{n+1} + (\Delta z)_n]. \quad (20)$$

It should be pointed out that the application of the uniform wall heat flux boundary condition ($\partial\theta/\partial n = 1$ at wall) to the finite-difference equations leads to a system of equations with a singular tridiagonal coefficient matrix for equation (17). This difficulty can be overcome, for example, by modifying the finite-difference equation at the wall or by shifting grid points one-half an increment from the boundaries. By noting that $u = v = w_f = 0$ at wall, equation (17) becomes $\nabla^2\theta = 0$ giving the following finite-difference equation.

$$\theta_{i-1,j}^{(n)} + \theta_{i+1,j}^{(n)} + \theta_{i,j-1}^{(n)} + \theta_{i,j+1}^{(n)} - 4\theta_{i,j}^{(n)} = 0. \quad (21)$$

By applying the boundary condition $\partial\theta/\partial n = 1$ at wall, the wall temperature can be computed after the temperatures in the interior region are found. The accuracy of the numerical solution and computing time depend on the mesh size and the axial step size. The relaxation parameter used for equations (15) and (16) ranges from 1·0 to 1·5 depending on the value of Rayleigh number. A relaxation factor of 1·0 is used for higher Rayleigh number. The mesh size is established by convergence study. The mesh sizes used in the final computation and the typical computing times required on IBM360/67 in obtaining a complete result for the axial distance z ranging from 0·001 to 1·0 with a given value of Rayleigh number are given below:

γ	M	N	Time (min)
0·2	8	80	6
0·5	10	40	6
1	16	32	10
2	20	20	5
5	30	12	5

4. HEAT TRANSFER RESULTS

4.1 *Field characteristics*

Although presentation of local Nusselt numbers in the thermal entrance region is the major goal here, temperature distribution, axial temperature development and development of secondary flow pattern are of engineering interest, and useful in clarifying the heat transfer mechanism. The temperature profiles along the vertical and horizontal center lines at various axial positions are shown in Fig. 2 for the case of $\gamma = 1$ and $Ra = 3 \times 10^4$. The gradual development of the temperature profile is clearly seen and the temperature gradient normal to the wall is seen to be constant. For the uniform wall heat flux boundary condition under consideration, the wall temperature distribution is of practical interest in design. Figure 3 shows the wall temperature distributions at various axial positions for the case of $\gamma = 1$ and $Ra = 3 \times 10^4$. For the rectangular channel, hot spots appear at the corners and the wall temperature is seen to be highest at the upper corner. The secondary flow plays an important role in the thermal entrance region heat transfer and the secondary flow

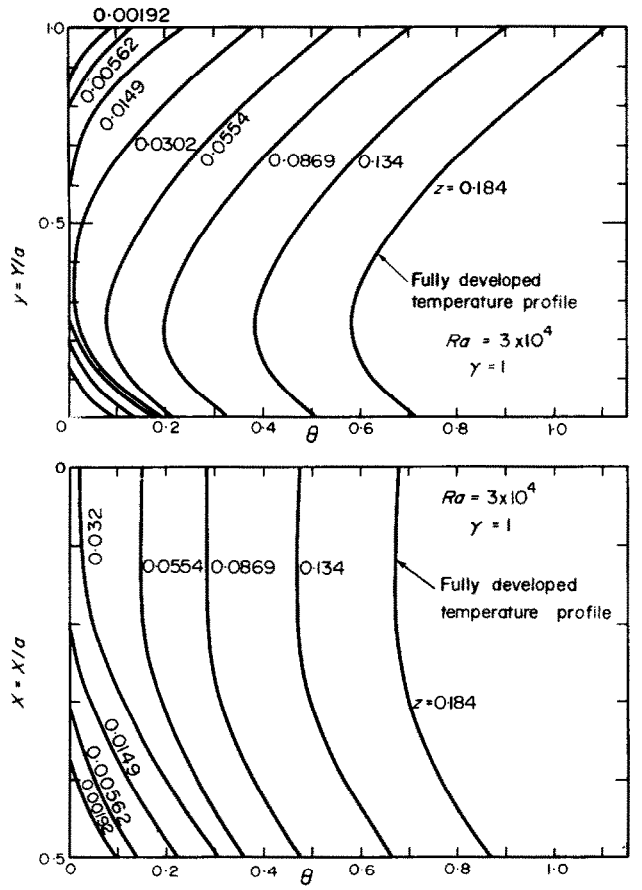

FIG. 2. Temperature distributions at $X = 0$ and $Y = b/2$ in the thermal entrance region of square channel with $Ra = 3 \times 10^4$.

patterns at six axial positions are shown in Fig. 4(a) and (b) for the case of $\gamma = 1$ and $Ra = 3 \times 10^4$. The maximum value of the stream function represents the intensity of the secondary flow and the movement of the location of the maximum stream function along the axial direction is also of interest. Figure 4 shows that the value of the maximum stream function at any given cross-section increases gradually from the value zero at the entrance $z = 0$ to a maximum value at some distance from the entrance and then decreases further along the axial direction until the fully developed temperature profile is reached. Noting that the secondary flow is caused by temperature gradient $\partial\theta/\partial x$ normal to the vertical wall as indicated in equation (15), the above phenomenon can be explained, for example, from the temperature distributions along the horizontal central line shown in Fig. 2. In Fig. 2, the temperature difference between the mid-point of side wall and the centre of the channel is seen to be greater at $z = 0{\cdot}0302$ than those at $z = 0{\cdot}0149$ and $0{\cdot}0554$. This observation can be contrasted to the secondary flow patterns for $z = 0{\cdot}0149$, $0{\cdot}0302$ and $0{\cdot}0554$ shown in Fig. 4. The centres of the secondary flow are seen to move toward the bottom and side walls along the axial direction.

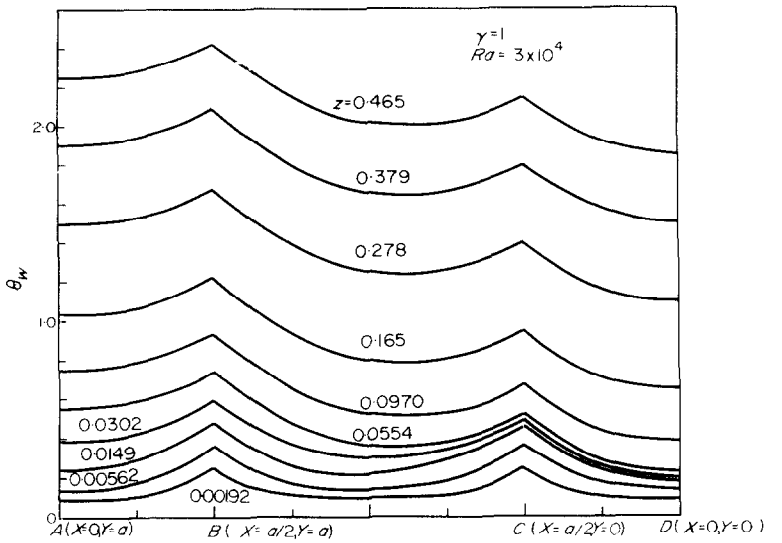

FIG. 3. Wall temperature distributions in the thermal entrance region of square channel with $Ra = 3 \times 10^4$.

A series of patterns for isothermals from $z =$ 0·00562 to $z = 0{\cdot}165$ is shown in Fig. 5(a) and (b) to illustrate the entrance effect on isothermals. The locations of the eyes of the vortices and the values for maximum stream functions are also shown for reference. Near the entrance $z =$ 0·00562, the secondary flow is still weak and the isothermals are seen to be nearly symmetric with respect to both the horizontal and vertical center lines. The increasing distortion of the

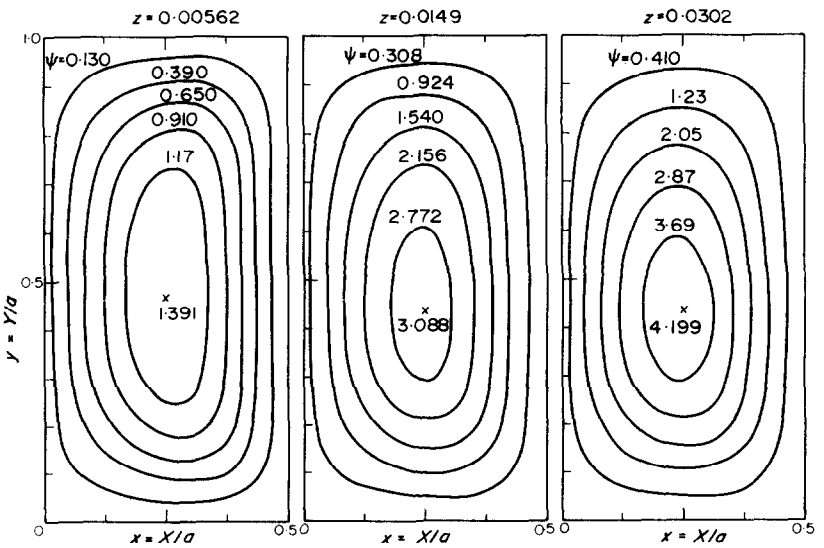

FIG. 4(a). Streamlines for secondary flow at $z = 0{\cdot}00562$, 0·0149 and 0·0302 for square channel with $Ra = 3 \times 10^4$.

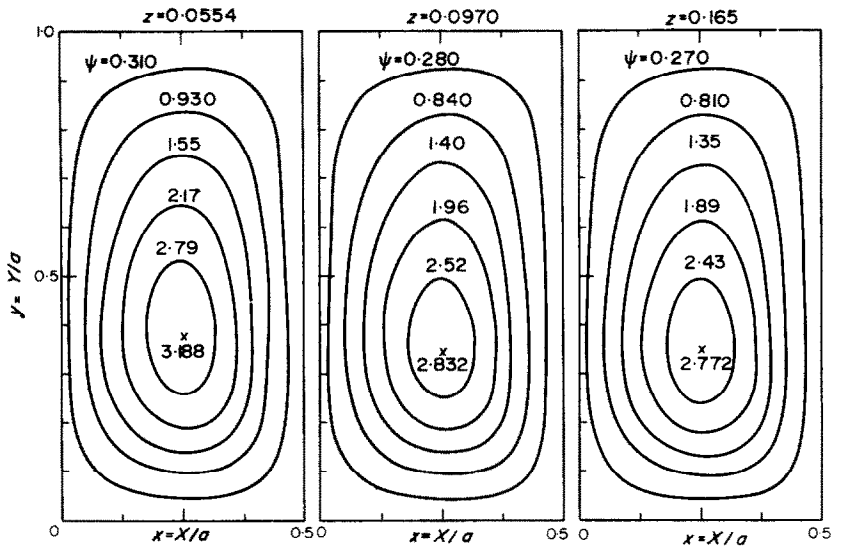

FIG. 4(b). Streamlines for secondary flow at $z = 0{\cdot}0554$, $0{\cdot}0970$ and $0{\cdot}165$ for square channel with $Ra = 3 \times 10^4$.

pattern for isothermals along the axial distance can also be seen from the movement of the location of minimum temperature toward the lower wall. The increase of the secondary flow intensity with the distance from the entrance and subsequent decrease after reaching a maximum can also be explained from a series of patterns shown in Fig. 5. The temperature distributions across the cross-section shown in Fig. 2 can be contrasted to a series of patterns for isothermals shown

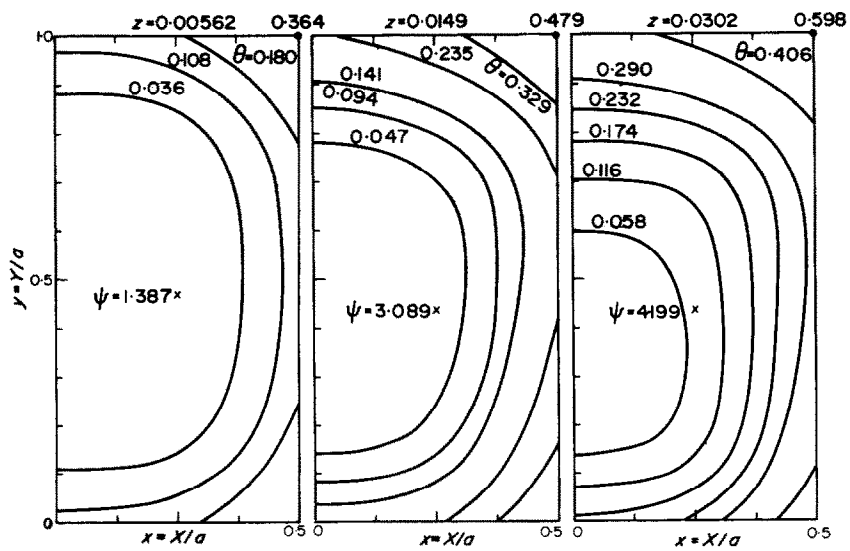

FIG. 5(a). Isothermals at $z = 0{\cdot}00562$, $0{\cdot}0149$ and $0{\cdot}0302$ for square channel with $Ra = 3 \times 10^4$.

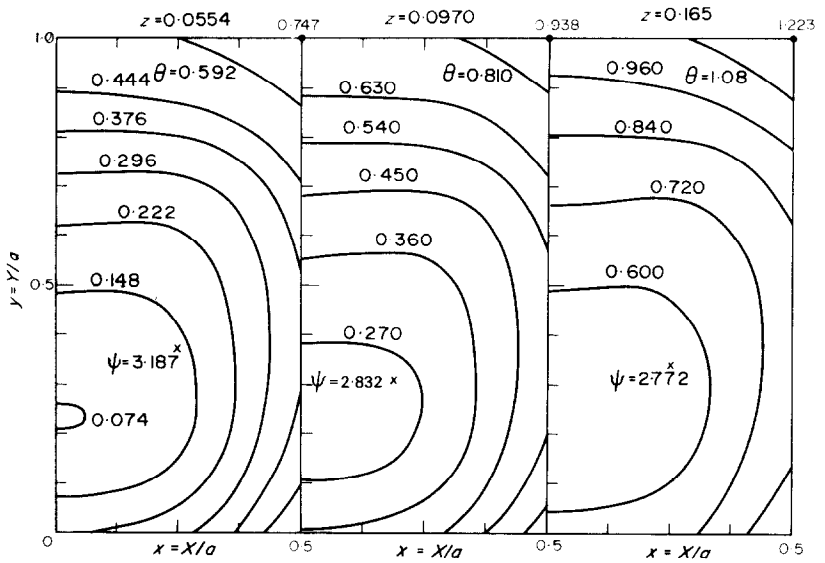

FIG. 5(b). Isothermals at $z = 0{\cdot}0554, 0{\cdot}0970$ and $0{\cdot}165$ for square channel with $Ra = 3 \times 10^4$.

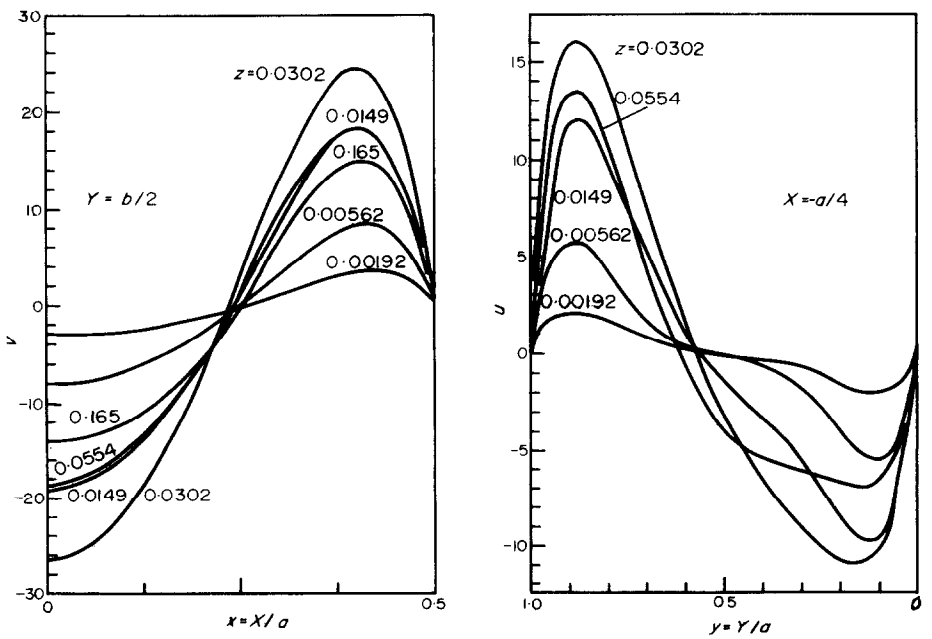

FIG. 6. Secondary flow velocity distributions at $Y = b/2$ and $X = -a/4$ for square channel with $Ra = 3 \times 10^4$.

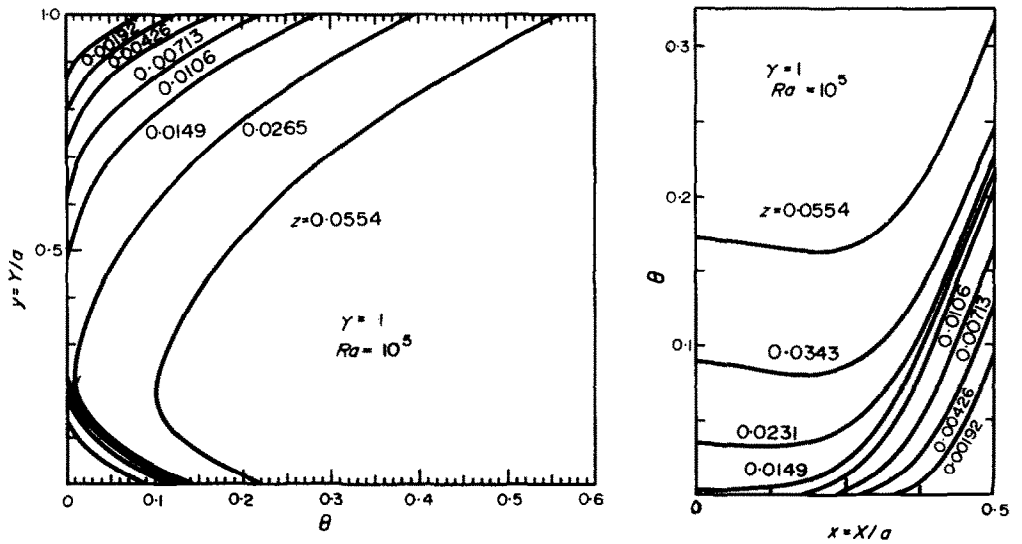

FIG. 7. Temperature distributions at $X = 0$ and $Y = b/2$ in the thermal entrance region of square channel with $Ra = 10^5$.

in Fig. 5. In Fig. 5, the isothermals for smaller values of θ in the central core are not shown since the temperatures are fairly uniform there.

The distributions of secondary velocity components, v along $Y = b/2$ and u along $X = -a/2$, are shown in Fig. 6 for the case $\gamma = 1$ and $Ra = 3 \times 10^4$. The increase and subsequent decrease of the secondary flow intensity along the axial direction can be seen clearly. The distribution for u is nearly symmetric about the horizontal central axis $Y = b/2$ at $z = 0{\cdot}00192$ but symmetry is gradually destroyed as the distance from the entrance increases further.

The effect of Rayleigh number on axial temperature profile development is of considerable interest. The temperature profiles corresponding to those shown in Fig. 2 are illustrated in Fig. 7 for the case of $\gamma = 1$ and $Ra = 10^5$ for comparison. It is seen that as Rayleigh number increases the temperature difference between the top and bottom plates increases. This situation implies that thermal instability problem [10, 11] may arise for a horizontal rectangular channel with large aspect ratio. Furthermore, the temperature distribution along the horizontal central axis exhibits negative temperature gradient $\partial\theta/x$ in the central region after reaching $z \approx 0{\cdot}0231$. This phenomenon also contributes to the decrease of the intensity for secondary flow. Although not presented here, the intensity of the secondary flow indeed decreases after reaching $z = 0{\cdot}0149$ for the case $\gamma = 1$ and $Ra = 10^5$. With the presentation of the pertinent field characteristics completed, the variation of the Nusselt number in the thermal entrance region will be considered next.

4.2 *Nusselt number*

The Nusselt number may be determined from the definition based on the temperature gradient at the wall or using the overall energy balance for the axial length dZ. The results are:

$$Nu = \bar{h}D_e/k$$

$$(Nu)_1 = 1/\overline{[w(\bar{\theta}_w - \theta)]} \qquad \text{with } \bar{w} = 1 \quad (22)$$

$$(Nu)_2 = \overline{w(\partial\theta/\partial z)}/4\overline{[w(\theta_w - \theta)]}. \quad (23)$$

Simpson's rule is used in computing the average quantities indicated above. The above two alternative expressions for the local Nusselt

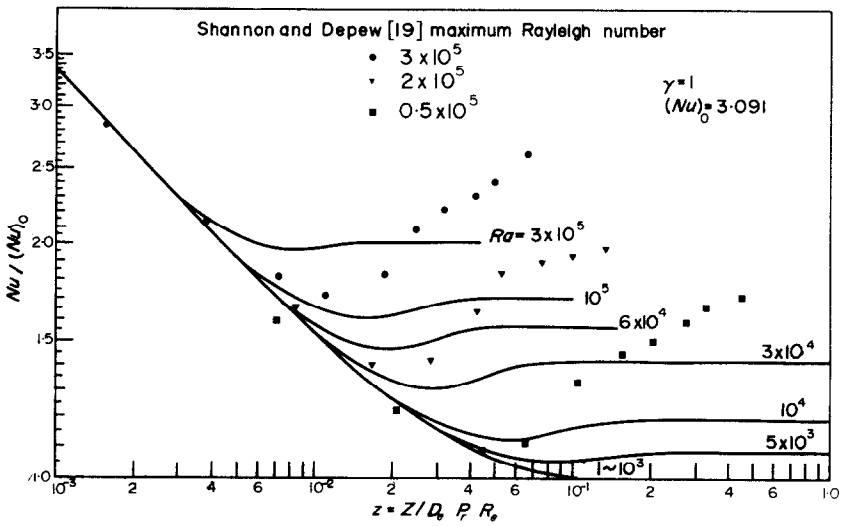

FIG. 8. Local Nusselt number variation for square channel with Ra as parameter and comparison with experimental data from Shannon and Depew [19] for circular tube.

number afford checking the convergence of the heat transfer results. Usually the first three figures check and the average of $(Nu)_1$ and $(Nu)_2$ is taken as the value for the Nusselt number.

4.3 *Nusselt number result*

Figure 8 presents the local Nusselt number variation in the form of $Nu/(Nu)_0$ versus dimensionless axial distance z for a horizontal square channel ($\gamma = 1$) with Rayleigh number as parameter. It is seen that the buoyancy effect is practically negligible when $Ra < 10^3$. The present problem without buoyancy effect for a square channel has been solved by Sparrow and Siegel [12] and Hicken [13] using a variational method. However, the Nusselt number result in the thermal entrance region is not available for direct comparison with the present numerical result. The present numerical result checks exactly with the known limiting Nusselt number $(Nu)_0 = 3{\cdot}091$ [14, 15] for the fully developed case confirming the accuracy and convergence of the present numerical solution. For a given Rayleigh number greater than say 10^3, the secondary flow effect appears at a certain distance z from the entrance depending on the magnitude of Rayleigh number. For each curve shown in Fig. 8, a minimum local Nusselt number exists. The location of the minimum Nusselt number is closely related to the appearance of the maximum secondary flow intensity which can be checked by examining Figs. 4 or 5. The occurrence of minimum Nusselt number is a result of combined entrance and secondary flow effects and the phenomenon is analogous to the entrance region Nusselt number variations presented by Linke and Kunze [16] and Mills [17] for the developing turbulent flow in a uniformly heated tube. It is noted that the dip in the curves for local Nusselt numbers near the entrance with simultaneous development of turbulent flow and temperature field can be explained by the fact that the boundary layers along the tube walls are at first laminar and subsequently change to turbulent flow through a transition region. A similar dip in the curve which coincides with the occurrence of a transition from laminar to turbulent flow appears also in the experimental

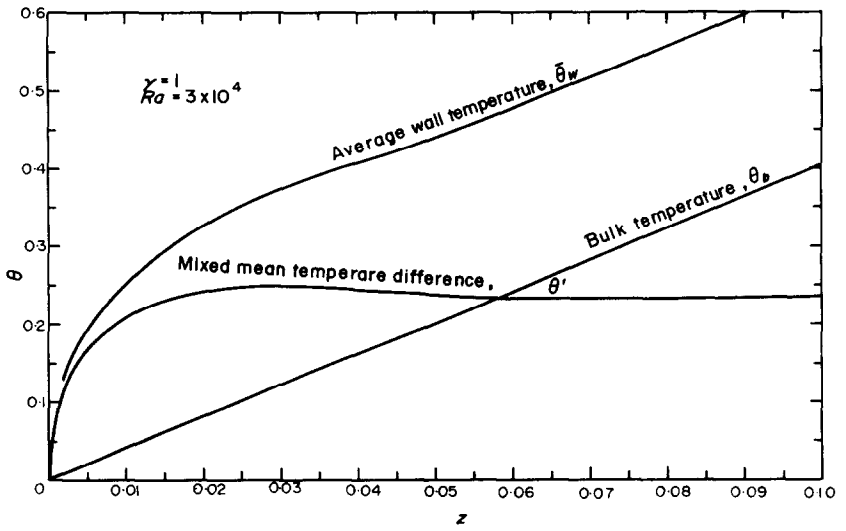

FIG. 9. Axial distributions for average wall temperature, bulk temperature and mixed mean temperature difference for square channel with $Ra = 3 \times 10^4$.

results for the case of horizontal isothermal tube presented by Jackson, Purdy and Oliver [18].

The question arises as to why the local Nusselt number increases after reaching a minimum value and subsequently approaches an asymptotic limiting value when the temperature profile becomes fully developed. This question can be answered by examining the definition of the Nusselt number and the variation of mixed mean temperature difference $\theta' = \iint_A w(\bar{\theta}_w - \theta)\,dxdy / \iint_A w\,dxdy$ along the axial distance as shown in Fig. 9. The variations of the average wall temperature $\bar{\theta}_w$ and the bulk temperature $\theta_b = \iint_A w\theta\,dxdy / \iint_A w\,dxdy$ along the axial distance are also shown in Fig. 9 for reference.

The experimental data are apparently not available for comparison with the numerical results presented in Fig. 8. However, it is instructive to compare the present numerical results for square channel with the experimental data obtained by Shannon and Depew [19] using water for combined free and forced laminar convection in a horizontal tube with uniform wall heat flux. In making the comparison between the numerical and experimental results shown in Fig. 8, it should be pointed out that Shannon and Depew [19] used the maximum Rayleigh number based on the temperature difference $(\bar{T}_w - T_b)$ [19] as a parameter whereas the Rayleigh number in this work is based on the characteristic temperature $\theta_c = q_w D_e/k$. Consequently, the direct comparison is not possible. Although the present theory is based on large Prandtl number assumption, a study of the implication of the large Prandtl number [4] leads one to believe that the present numerical results are valid also for water. In spite of the difference in geometrical shape between square channel and circular tube, the local Nusselt number results shown in Fig. 8 are seen to be qualitatively similar. The curve for pure forced convection is seen to check well with the experimental data from circular tube.

Recently, Muntjewerf, Leniger and Beek [20] presented the experimental results for local Nusselt number variation in the thermal entrance region of the uniformly heated vertical flat rectangular ducts and the variations in the local

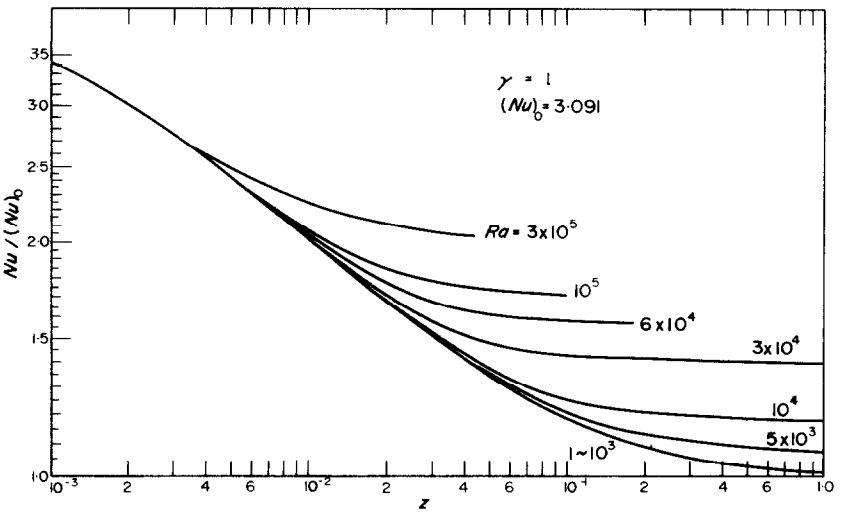

FIG. 10. Average Nusselt numbers vs. z for square channel with Rayleigh number as parameter.

Nusselt number are again seen to be similar to the numerical results shown in Fig. 8.

The average Nusselt number (overall value to an axial position z) variations along the entrance distance z corresponding to the Rayleigh numbers shown in Fig. 8 are plotted in Fig. 10. With the average Nusselt number, the dip in the curve for the local Nusselt number is smoothed out.

The effect of the aspect ratio of a rectangular channel on heat transfer result is of practical interest. The local Nusselt number variations in the thermal entry region for the aspect ratios $\gamma = 2$, 5, 0·5 and 0·2 are shown in Figs 11–14, respectively, with Rayleigh number as parameter. In each of these figures, the lowest curve can be regarded as a limiting case for pure forced

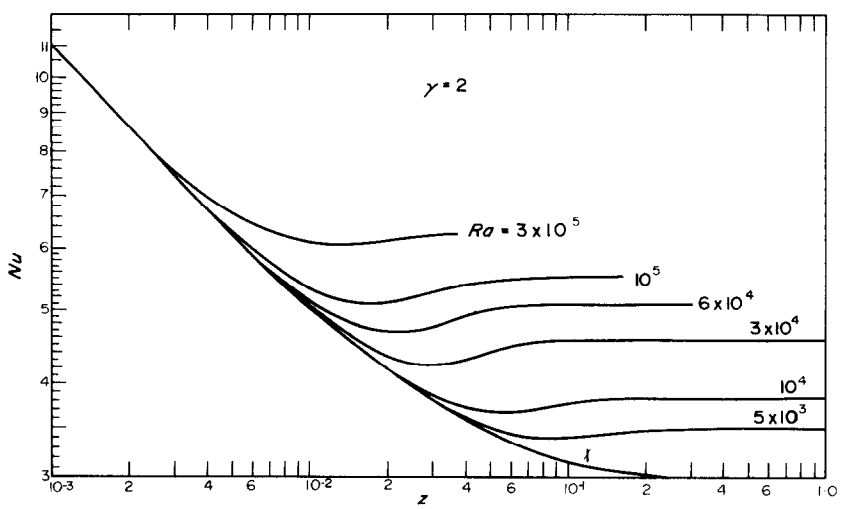

FIG. 11. Local Nusselt numbers vs. z for rectangular channel with aspect ratio $\gamma = 2$ for various Rayleigh numbers.

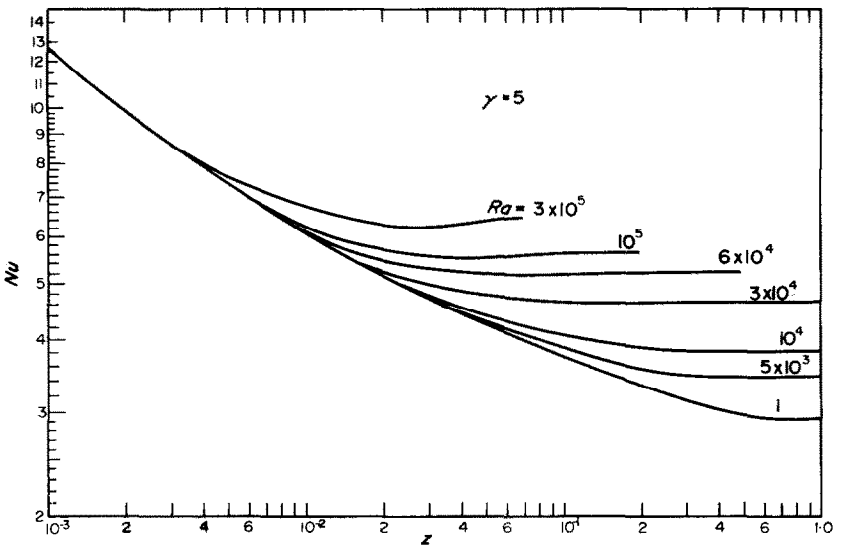

FIG. 12. Local Nusselt numbers vs. z for rectangular channel with aspect ratio $\gamma = 5$ for various Rayleigh numbers.

convection (Graetz problem). Within the range of Rayleigh numbers under investigation, the dip in the curves due to secondary flow becomes less obvious for the aspect ratios $\gamma = 5$, 0·5 and 0·2. It is noted that for the curves $Ra = 3 \times 10^5$ shown in Figs. 8–13, the numerical solution diverges beyond the axial distance shown in each figure. The exact values for the limiting Nusselt number $(Nu)_0$ for the fully developed case are not known for the aspect ratios other than one. The lowest curves shown in Figs. 10 and 12 are seen to approach the same limiting value of 3·0 at $z = 0{\cdot}306$.

The heat transfer results presented in Figs.

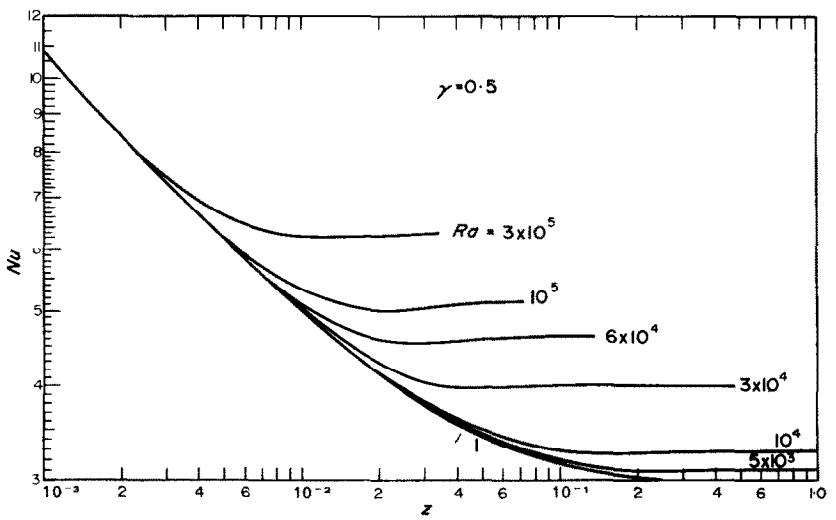

FIG. 13. Local Nusselt numbers vs. z for rectangular channel with aspect ratio $\gamma = 0{\cdot}5$ for various Rayleigh numbers.

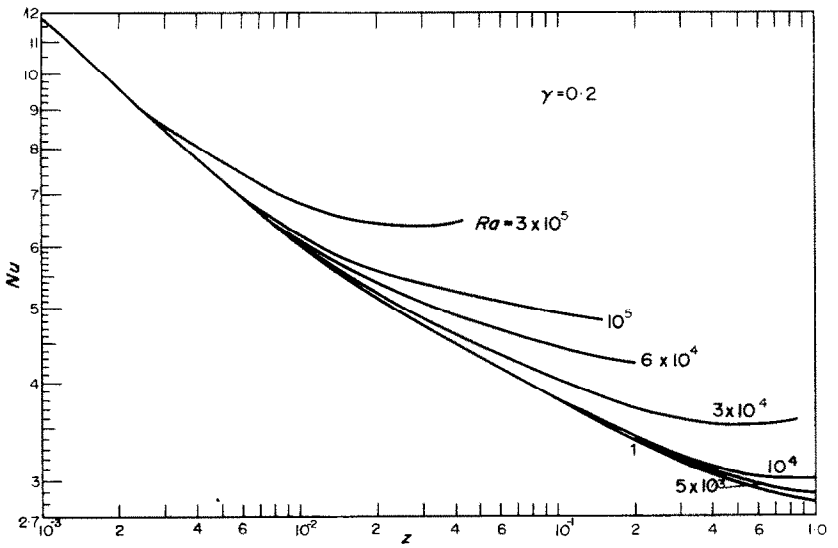

FIG. 14. Local Nusselt numbers vs. z for rectangular channel with aspect ratio $\gamma = 0{\cdot}2$ for various Rayleigh numbers.

8–14 show clearly that the effect of secondary flow represented by Rayleigh number is to decrease the thermal entrance length and increase the average heat transfer coefficient. The classical Graetz problem is clearly a limiting case, and is valid only when Rayleigh number is less than say 10^3 for the present problem.

5. CONCLUDING REMARKS

The classical Graetz problem for laminar forced convection in horizontal rectangular channels with uniform wall heat flux is extended by taking buoyancy effects into consideration. The Graetz problem with buoyancy effects valid for all Prandtl numbers is formulated, and the limiting case of large Prandtl is solved numerically.

The heat transfer results presented are believed to be valid for Prandtl number ranging from order 10 to infinity. It is pointed out that the classical Graetz problem is a limiting case, and is valid only when Rayleigh number is less than say 10^3. This remark is considered to be valid also for other various noncircular channels or circular ducts. Although this investigation is concerned with the uniform wall heat flux case, solutions for uniform wall temperature can be obtained by the same method. Furthermore, solutions for inclined channel case can also be approached by a numerical method.

The variation of local Nusselt number along the channel for uniform wall heat flux shows that buoyancy effect is negligible up to a certain entry length z depending on the magnitude of the Rayleigh number. The curve for Nusselt number for each Rayleigh number then branches out from the curve for pure forced convection and after reaching a minimum value approaches a limiting value when the temperature profile becomes fully developed. The dip in the curves for local Nusselt number is similar to that reported in the literature for the case of developing turbulent heat transfer in the thermal entrance region of a pipe with uniform wall heat flux. The effect of buoyancy forces is to decrease the thermal entrance length and increase the average heat transfer coefficient. At higher Rayleigh number, the temperature profile develops rapidly.

The definition of Rayleigh number based on $(\bar{T}_w - T_b)$ is variable in the thermal entrance region. In contrast, the present definition based on characteristic temperature $\theta_c = q_w D_e/k$ is a constant, and convenient for design. Finally, one additional reference [21] that is pertinent to the present problem is included here for completeness.

ACKNOWLEDGEMENT

The authors wish to acknowledge the support of the National Research Council of Canada through grant NRC A1655 for this research.

REFERENCES

1. L. GRAETZ, Über die Wärmeleitungsfahigkeit von Flüssigkeiten, *Ann. Phys.* **25**, 337–357 (1885).
2. C. J. HSU, An exact analysis of low Peclet number thermal entry region heat transfer in transversely nonuniform velocity fields, *A.I.Ch.E. Jl* **17**, 732–740 (1971).
3. C. A. DEPEW and S. E. AUGUST, Heat transfer due to combined free and forced convection in a horizontal and isothermal tube, *J. Heat Transfer* **93**, 380–384 (1971).
4. K. C. CHENG, G. J. HWANG and M. AKIYAMA, On a simple correlation for Prandtl number effect on forced convective heat transfer with secondary flow, *Int. J. Heat Mass Transfer* **15**, 172–175 (1972).
5. G. J. HWANG, Thermal instability and finite amplitude convection with secondary flow, Ph.D. thesis, Dept. of Mechanical Engineering, University of Alberta, Edmonton, Alberta, Canada (1970).
6. G. J. HWANG and K. C. CHENG, Boundary vorticity method for convective heat transfer with secondary flow-application to the combined free and forced laminar convection in horizontal tubes, *Heat Transfer 1970*, Proc. Fourth International Heat Transfer Conference, vol. 4, NC 3.5. Elsevier Publishing Company, Amsterdam (1970).
7. K. C. CHENG and M. AKIYAMA, Laminar forced convection heat transfer in curved rectangular channels, *Int. J. Heat Mass Transfer* **13**, 471–490 (1970).
8. S. D. CONTE and R. T. DAMES, An alternating direction method for solving the biharmonic equation, *Math. Tables Aids Comput.* **12**, 198–205 (1958).
9. D. YOUNG, The numerical solution of elliptic and parabolic partial differential equations, *Survey of Numerical Analysis*, edited by J. TODD, pp. 380–438. McGraw-Hill, New York (1962).
10. W. NAKAYAMA, G. J. HWANG and K. C. CHENG, Thermal instability in plane Poiseuille flow, *J. Heat Transfer* **92**, 61–68 (1970).
11. M. AKIYAMA, G. J. HWANG and K. C. CHENG, Experiments on the onset of longitudinal vortices in laminar forced convection between horizontal plates, *J. Heat Transfer* **93**, 335–341 (1971).
12. E. M. SPARROW and R. SIEGEL, Application of variational methods to the thermal entrance region of ducts, *Int. J. Heat Mass Transfer* **1**, 161–172 (1960).
13. E. HICKEN, Das Temperaturfeld in laminar durchströmten Kanälen mit Rechteck-Querschnitt bei unterschiedlicher Beheizung der Kanalwände, *Wärme-und Stoffübertragung* **1**, 98–104 (1968).
14. E. M. SPARROW and R. SIEGEL, A variational method for fully developed laminar heat transfer in ducts, *J. Heat Transfer* **81**, 157–167 (1959).
15. K. C. CHENG, Laminar forced convection in regular polygonal ducts with uniform peripheral heat flux, *J. Heat Transfer* **91**, 156–157 (1969).
16. W. LINKE und H. KUNZE, Druckverlust und Warmeübergang im Anlauf der turbulenten Rohrströmung, *Allgem. Wärmetech.* **4**, 73–79 (1953).
17. A. F. MILLS, Experimental investigation of turbulent heat transfer in the entrance region of a circular duct, *J. Mech. Engng Sci.* **4**, 63–77 (1962).
18. T. W. JACKSON, K. R. PURDY and C. C. OLIVER, The effects of resonant acoustic vibrations on the Nusselt numbers for a constant temperature horizontal tube, *International Developments in Heat Transfer*, Procs. 1961–62 Heat Transfer Conference, ASME (1963).
19. R. L. SHANNON and C. A. DEPEW, Combined free and forced laminar convection in a horizontal tube with uniform heat flux, *J. Heat Transfer* **90**, 353–357 (1968).
20. A. K. MUNTJEWERF, H. A. LENIGER and W. J. BEEK, An experimental investigation of heat transfer to laminar Newtonian flows in uniformly heated vertical flat rectangular ducts, *Appl. Sci, Res.* **23**, 134–146 (1970).
21. R. L. SHANNON and C. A. DEPEW, Forced laminar flow convection in a horizontal tube with variable viscosity and free-convection effects, *J. Heat Transfer* **91**, 251–258 (1969).

INFLUENCE DES FORCES D'ARCHIMEDE SUR LE TRANSFERT THERMIQUE LAMINAIRE DANS LA REGION D'ENTREE DE CANAUX RECTANGULAIRES HORIZONTAUX AVEC UN FLUX THERMIQUE PARIETAL UNIFORME ET POUR UN FLUIDE A GRAND NOMBRE DE PRANDTL

Résumé—Le problème de Graetz pour un écoulement laminaire entièrement développé dans des canaux rectangulaires horizontaux avec flux thermique uniforme à la paroi est élargi en incluant l'effet des forces d'Archimède dans l'analyse pour un fluide à grand nombre de Prandtl. On présente une formulation générale valable pour tous les nombres de Prandtl et on aborde le cas limite des grands nombres de Prandtl par une

méthode numérique. Les développements typiques du profil de température, de la température pariétale et de l'écoulement secondaire dans la région d'entrée thermique sont présentées dans le cas d'un canal carré $\gamma = 1$. Les variations du nombre de Nusselt local sont présentées pour les rapports de forme $\gamma = 0.2$; 0.5; 1; 2; 5 et avec le nombre de Rayleigh pris comme paramètre. A cause de l'effet d'entrée et de l'écoulement secondaire, un nombre de Nusselt minimal apparaît à quelque distance de l'entrée, dépendant de la valeur du nombre de Rayleigh. Ce comportement est semblable à celui observé dans la région d'entrée thermique lorsqu'apparaît la transition laminaire-turbulent de l'écoulement. On voit que l'influence du nombre de Rayleigh diminue la longueur d'entrée thermique et que la solution de Graetz, laquelle néglige les forces d'Archimède, n'est applicable que lorsque le nombre de Rayleigh est inférieur à 10^3. Une étude de l'effet pratique du grand nombre de Prandtl sur les résultats de transfert thermique dans le développement hydrodynamique et thermique complet, revèle que les résultats présents de transfert thermique sont valables pour un nombre de Prandtl variant depuis 10 jusqu'à l'infini.

AUFTRIEBSEINFLÜSSE AUF DEN LAMINAREN WÄRMEÜBERGANG IM THERMISCHEN EINLAUFBEREICH EINES WAAGERECHTEN RECHTECKKANALS MIT EINHEITLICHEM WÄRMESTROM AN DER WAND FÜR FLÜSSIGKEITEN GROSSER PRANDTL-ZAHL

Zusammenfassung—Das Graetz-Problem für eingelaufene laminare Strömung in horizontalen rechteckigen Kanälen mit gleichmässiger Wärmestromdichte an der Wand wird erweitert im Hinblick auf den Einfluss der Auftriebskräfte bei Fluiden mit grosser Prandtl-Zahl. Eine allgemeine Formulierung wird vorgestellt die für alle Prandtl-Zahlen gültig ist. Der Grenzfall grosser Prandtl-Zahlen wird durch eine numerische Methode angenähert. Es werden die typischen Entwicklungen der Temperaturprofile, der Wandtemperatur, und der Sekundärströmung in der thermischen Einlaufstrecke dargestellt für den Fall des quadratischen Kanals $\gamma = 1$. Für die Seitenverhältnisse $\gamma = 0.2$; 0.5; 1; 2; und 5 werden örtliche Nusseltzahlen angegeben mit der Rayleigh-Zahl als Parameter. Die Einflüsse am Einlauf und die der Sekundärströmung bewirken ein Minimum der Nusselt-Zahl stromabwärts vom Eintritt abhängig von der Grösse der Rayleigh-Zahl. Dieses Verhalten ist ähnlich dem im thermischen Einlaufgebiet beim Umschlag von laminarer in turbulente Strömung. Der Einfluss der Rayleigh-Zahl liegt in Richtung einer Verkürzung der thermischen Einlauflänge. Die Graetz-Lösung, bei Vernachlässigung der Auftriebskräfte, ist nur anwendbar, wenn die Rayleigh-Zahl kleiner als etwa 10^3 ist. Untersucht man die praktischen Folgen grosser Prandtl-Zahlen auf den Wärmeübergang bei hydrodynamisch und thermisch voll ausgebildeter Strömung, so erkennt man, dass die vorliegenden Wärmeübergangsergebnisse gültig sind für Prandtl-Zahlen von 10 bis unendlich.

ВЛИЯНИЕ ПОДЪЕМНОЙ СИЛЫ НА ЛАМИНАРНЫЙ ПЕРЕНОС ТЕПЛА НА ТЕПЛОВОМ ВХОДНОМ УЧАСТКЕ ГОРИЗОНТАЛЬНЫХ ПРЯМОУГОЛЬНЫХ КАНАЛОВ С ОДНОРОДНЫМ ТЕПЛОВЫМ ПОТОКОМ НА СТЕНКЕ ПРИ БОЛЬШИХ ЧИСЛАХ ПРАНДТЛЯ

Аннотация—Задача Гретца для полностью развитого ламинарного течения в горизонтальных прямоугольных каналах с однородным тепловым потоком на стенке обобщается на случай больших чисел Прандтля с учетом влияния подъемной силы. Приводится общая формулировка задачи для произвольных чисел Прандтля. Численно решается предельный случай для большого числа Прандтля. Представлены типичные профили температуры стенки и вторичного течения на тепловом входном участке в квадратном канале $c\gamma = 1$. Представлены распределения локальных чисел Нуссельта для $\gamma = 0{,}2$; 0,5; 1; 2 и 5 с числом Релея в качестве параметра. В силу влияния вторичного течения минимальное число Нуссельта имеет место на некотором расстоянии от входа в зависимости от величины числа Релея. Зта ситуация подобна той, которая наблюдается на тепловом входном участке, где происходит переход ламинарного течения в турбулентное. Влияние числа Релея выражается в уменьшении длины теплового начального участка. Найдено что решение Гретца, пренебрегающее влиянием подъемной силы, годится для числа Релея меньше 10^3. Анализ влияния больших чисел Прандтля на теплообмен для случая гидродинамически и термически полностью развитого течения показывает, что полученные данные по теплообмену практически справедливы для диапазона чисел Релея от 10 до бесконечности.